The influence of the porous structure of anodic alumina on the formation and properties of germanium nanostructures

2016 Mater. Res. Express 3 015902

(http://iopscience.iop.org/2053-1591/3/1/015902)

Materials Research Express

RECEIVED
29 October 2015

REVISED
19 November 2015

ACCEPTED FOR PUBLICATION
18 December 2015

PUBLISHED
18 January 2016

PAPER

The influence of the porous structure of anodic alumina on the formation and properties of germanium nanostructures

R Valeev[1], **A Beltiukov**[1], **V Mukhgalin**[1] **and R Zakirova**[2]

[1] Physical-Technical Institute of UB RAS, Kirova str. 132, Izhevsk, 426000 Russia
[2] Udmurt State University, Universitetskaya str. 1, Izhevsk, 426034 Russia

E-mail: rishatvaleev@mail.ru

Keywords: porous Al_2O_3, germanium nanostructures, structural properties

Abstract

The influence of the porous structure of anodic alumina matrices on the structural and morphological properties of germanium nanostructures, obtained by high vacuum thermal deposition on anodic alumina, is reported. Scanning electron microscopy micrographs reveal the formation of Ge nanostructures in the form of rods and tubes with diameters from 16–130 nm and arrangements specified by the geometry characteristics of the porous matrix structure. X-ray diffraction and Raman scattering studies show the formation of nanostructures with structural states specified by the temperature of the substrate: the amorphous state at 200 °C and 300 °C, the mixed amorphous–crystalline state at 400 °C and the crystalline state at 500 °C. Germanium nanostructures with ordered distributions in the dielectric matrices are desired for application in optoelectronic devices.

1. Introduction

Germanium nanostructures in dielectric matrices, for example, SiO_2 and Al_2O_3, due to the size-defined possibility of high indirect optical transitions leading to strong lines and intensive blue photoluminescence in the visible region, could be useful for optoelectronic devices [1–6]. In addition to the size effect (quantum confinement), the influence on the appearance of luminescent properties may cause the formation of germanium oxides in the semiconductor–dielectric interface [2, 7], and the possible mechanism for this has been discussed yet [3–6]. The methods used to synthesize nanocomposites of Ge in SiO_2 or Al_2O_3 matrices include germanium ion implantation [4], dc magnetron sputtering [6, 8], laser ablation [9], etc. However, nanoparticles obtained by these methods have non-uniform distributions in the dielectric matrices and a very high size dispersion.

Of particular interest are Ge nanoparticles deposited into porous anodic alumina (PAA). These nanochannel-array materials have fine, uniform channels of nanometer dimensions, and the structure of PAA can be described as a close-packed array of columnar cells, whose size and interval can be controlled by changing the forming conditions [11–13]. This fact allows one to produce ordered nanoparticles of different materials templated into PAA matrices. Ordered distributions can provide increased optical and electronic properties to materials due to the coherent summation of individual particle properties. In [10], well-ordered Ge quantum dot arrays on PAA film on Si substrates were obtained using a molecular beam epitaxy (MBE) process. Mei *et al* produced monocrystalline germanium nanorods and arrays on a PAA template using the saturated vapor adsorption method, during which the Ge gas pressure was saturated at a high temperature in an airtight quartz tube [14]. The MBE process mentioned above is the conventional method for producing electronic components, but is very complicated and requires ultra-high vacuum conditions, whereas the method described in [14] is difficult to insert into the existing microelectronic processing technology.

In this paper we propose using the thermal deposition method for the fabrication of germanium nanostructures embedded into PAA templates with different porous structures. These matrices, produced by the anodic oxidation process in oxalic acid solution, have a hexagonal ordered distribution vertically oriented to the surface of the uniform matrix pores [11–13]. The main stages of the growing nanostructures in the crystalline

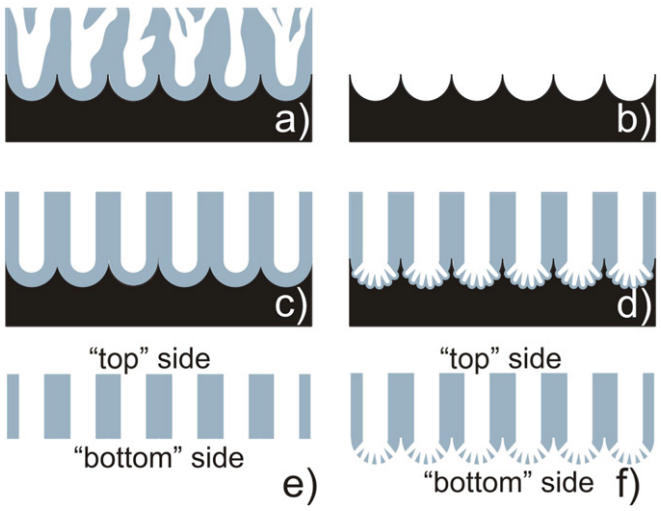

Figure 1. Schematic drawings of the two-step anodization process. (a) The formation of PAA with random pore nucleation; (b) Al substrate after etching of the PAA formed during the first anodization process; (c) PAA after a second anodization with highly ordered hexagonal porous structures (without stepwise establishment of anodization potential); (d) PAA after a second anodization with highly ordered hexagonal porous structures (with stepwise establishment of anodization potential); (e) PAA template after chemical etching of aluminum and barrier layer for samples synthesized without stepwise establishment of anodization potential; and (f) PAA template after chemical etching of aluminum and barrier layer for samples synthesized with stepwise establishment of anodization potential.

and amorphous states are determined. The influence of the pore distribution and size of the matrices on the morphology of the germanium nanoparticles is also established. The size, distribution and form of the obtained germanium nanostructures suggest their possible application in infrared detectors with ultra-high resolution or in highly efficient light sources.

2. Experimental details

PAA templates with a highly ordered porous structure were prepared using the two-stage anodization technique described in [11–13]. Prior to anodization, the aluminum plates were annealed at 550 °C for 24 h in air in order to remove any mechanical stress and enhance the grain size in the metal. Plates were produced by multiple rolling of high purity (99.99%) aluminum pellets to a thickness of 0.5 mm. Subsequently, the Al plates were electrochemically polished to a mirror finish and cleaned repeatedly with acetone and deionized water under sonication. Anodization was carried out in a two-electrode cell in 0.3 M oxalic acid (98%, Aldrich) at 40, 80 and 120 V using a Pt wire as a counter electrode. During anodization the electrolyte temperature was about 0 °C. To avoid electric breakdown, a voltage of 120 V was established stepwise with a step of 0.6 V. After anodization the aluminum plate and a barrier layer of alumina were removed. Germanium was deposited on the 'top' and 'bottom' of the templates (figure 1). It should be noted that the 'bottom' of the matrix synthesized at 120 V has a more complicated morphology (see figure 1(f)). This is caused by the formation of a greater number of small pores in the initial stage of oxidation during the stepwise increase of the anodization potential at the second step of the anodization process.

The deposition of germanium was carried out in an ultra-high (no higher than 10^{-8} Pa) vacuum thermal deposition chamber mounted on a LAS-2000 (Riber, France) device. The PAA matrices and smooth α-Al_2O_3 substrates (hereafter substrates) were mounted on a holder equipped with heating and cooling systems [15]. Germanium films deposited on smooth α-Al_2O_3 were used as the reference standard. Prior to deposition the substrates were heated for 5 h at 400 °C to remove gases and water adsorbed in pores. Ge evaporation was carried out from a molybdenum crucible heated to 1280 °C at substrate temperatures of 25 °C, 200 °C, 300 °C, 400 °C and 500 °C. The film growth rate was about 100 Å s^{-1}.

The surface morphology was studied using an atomic force microscope (AFM; SOLVER P47, NT-MDT, Russia) and a scanning electron microscope (SEM) (Supra 50 VP, LEO) equipped with a energy-dispersive x-ray (EDX) analysis system (Oxford INCA Energy+).

X-ray diffraction (XRD) patterns were recorded in the 2θ range of 20°–60° using a BRUKER D8 Advance X-ray Diffractometer (Bruker ASX) under Cu–$K\alpha$ radiation in the grazing incidence angle mode using a single Gobel mirror; the incident angle was 0.2°. The signal was recorded for 10 s per point. The treatment of the

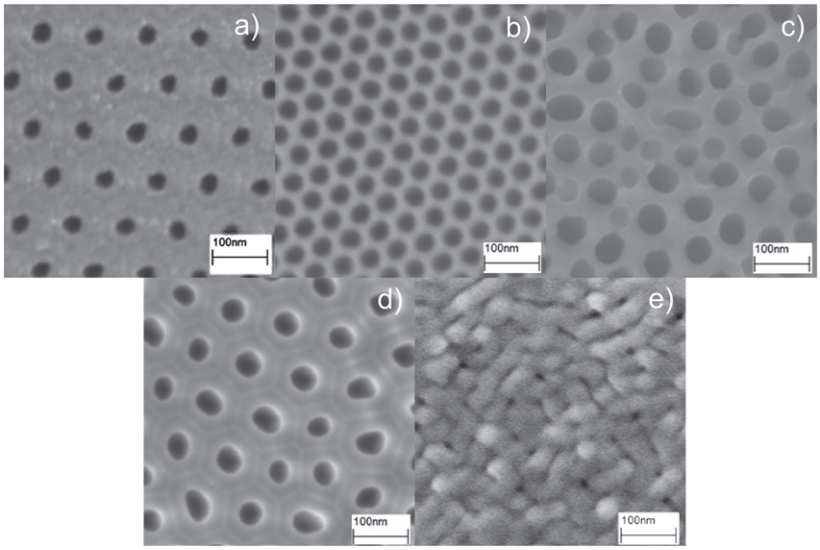

Figure 2. SEM images of the initial PAA matrices. d is the average diameter of the pores and l is the average distance between the pore centers. (a) PAA40^{bot} ($U = 40$ V, $d = 43 \pm 4$ nm, $l = 100 \pm 10$ nm); (b) PAA40^{bot}_5 ($U = 40$ V, after etching for 5 min in 5% H_3PO_4, $d = 67 \pm 5$ nm, $l = 100 \pm 10$ nm); (c) PAA80^{bot} ($U = 80$ V, $d = 94 \pm 12$ nm, $l = 220 \pm 12$ nm); (d) PAA120^{bot} ($U = 120$ V, $d = 140 \pm 20$ nm, $l = 290 \pm 20$ nm); and (e) PAA120^{top} ($U = 120$ V, $d = 15 \pm 2$ nm, $l = 37 \pm 2$ nm).

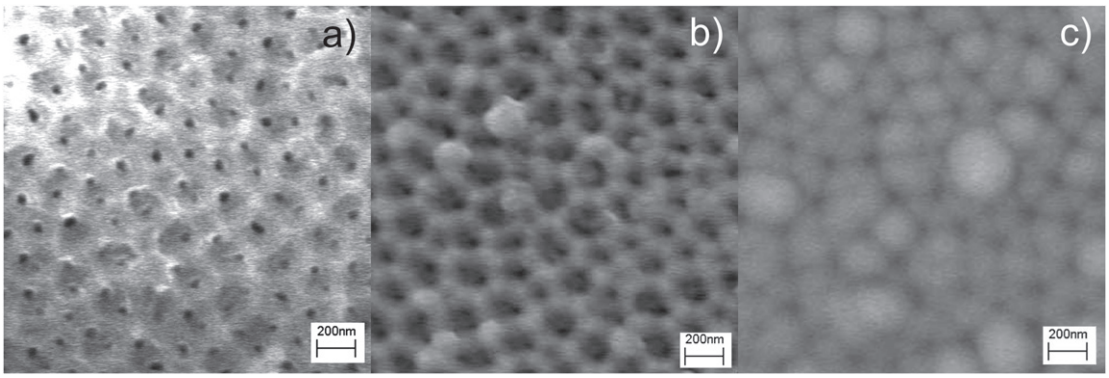

Figure 3. SEM images illustrating Ge growth on the PAA40^{bot} matrix after deposition of Ge corresponding to 10 nm (a), 100 nm (b) and 400 (c) nm film thicknesses on a smooth Al_2O_3 surface.

diffraction patterns was performed using the methods and programs described in [16]. A phase analysis was carried out using the JCPDS database.

Raman spectra were recorded by a Raman spectrometer (Centaur, Nano Scan Technology, Russia). For monochromatization of the incident beam a diffraction grid with 1200 bars per millimeter was used. Excitation was performed by a laser with $\lambda = 532$ nm and a power of 50 mW. A Raman signal was recorded for 0.3 s per point using a CCD matrix with cooling by Peltier elements to -40 °C.

3. Results and discussion

3.1. Formation and morphology

Germanium was deposited on the 'top' and 'bottom' of the PAA matrices. Figure 2 shows SEM images of the initial matrices synthesized under different anodization conditions.

It can be seen that the most ordered distribution of pores on the bottom is in the matrices obtained at 40 V (figure 2(a)). After etching for 5 min in 5% H_3PO_4 the average diameter of the pores increases, but the average distance between pore centers is retained (figure 2(b)). During the two-stage anodization of aluminum at 120 V with stepwise increasing of voltage, pores with small diameters are formed on the top of the matrix (figure 2(e)).

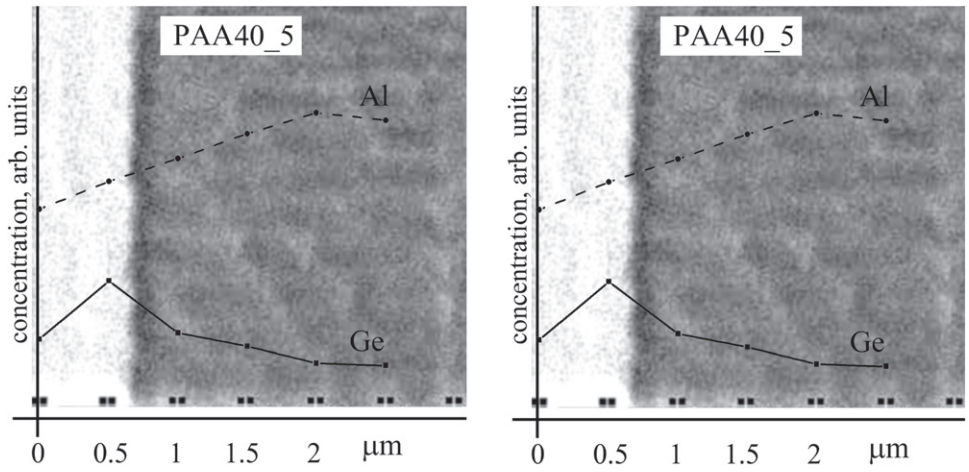

Figure 4. The depth distribution of germanium atoms in the pores of PAA matrices.

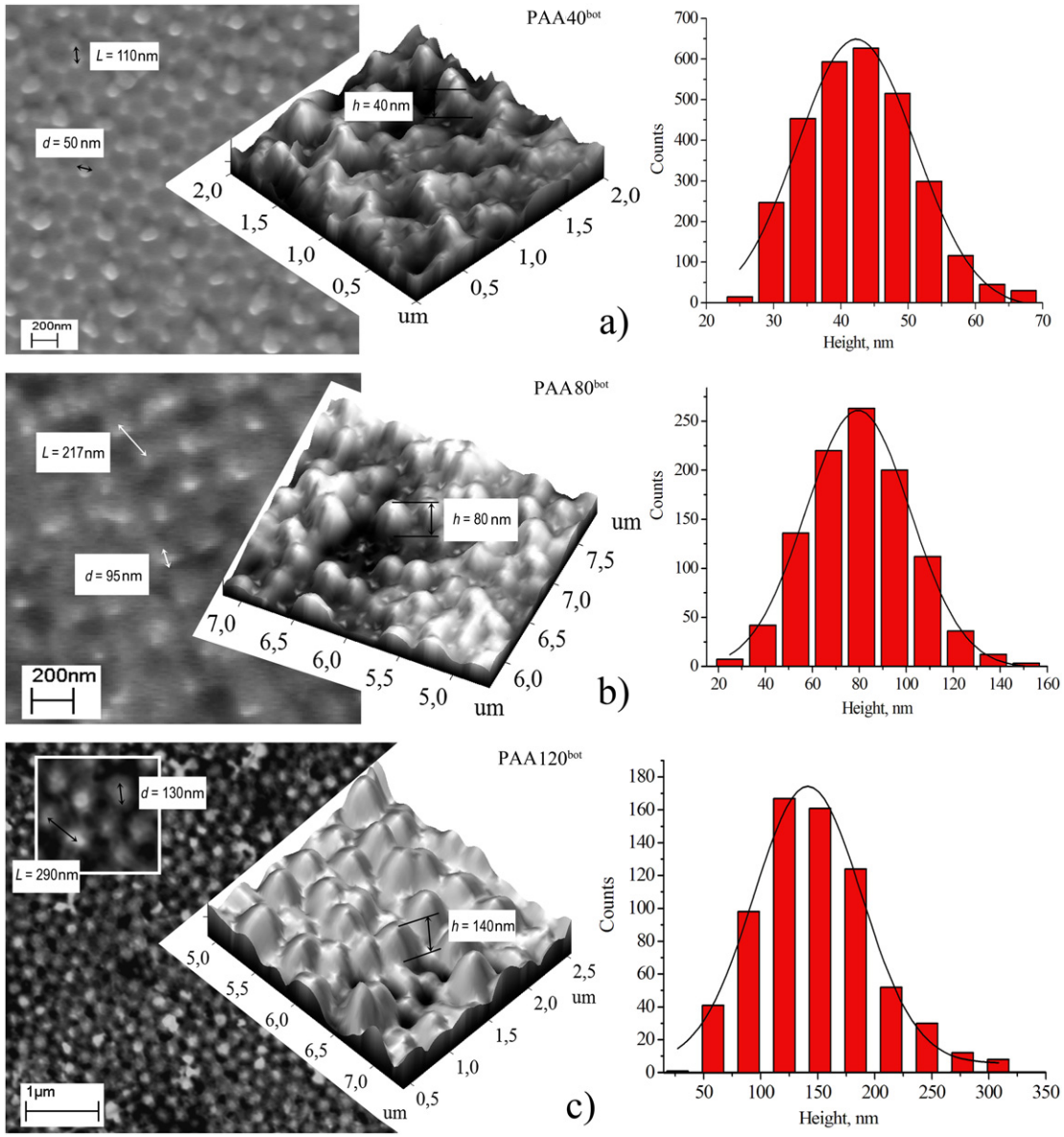

Figure 5. SEM and 3D AFM micrographs and histograms of the nanoparticle height distribution of Ge nanorods obtained by deposition on PAA40^{bot} (a), PAA80^{bot} (b) and PAA120^{bot} (c) after matrix etching.

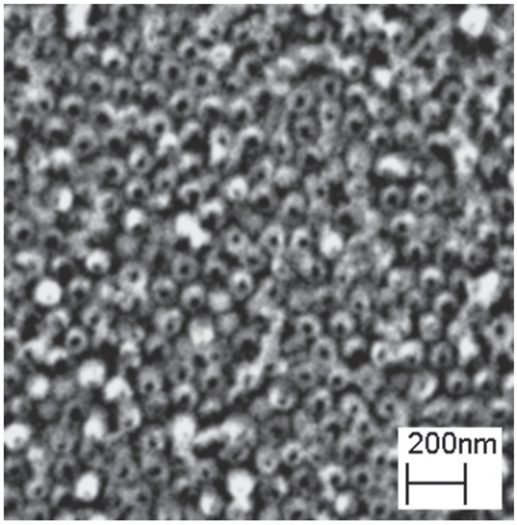

Figure 6. SEM micrograph of Ge nanorings obtained by deposition on PAA40^{bot}_5 after matrix etching.

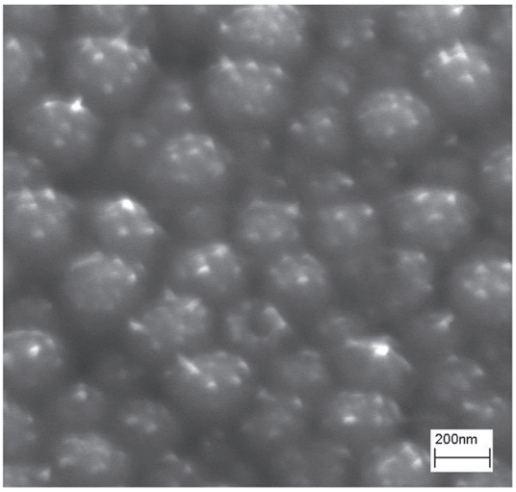

Figure 7. SEM micrograph of Ge nanostructures obtained by deposition on PAA120^{top} after matrix etching.

To investigate the process of germanium nanostructure growth, deposition on PAA matrix PAA40^{bot} was performed (figure 3). The process can be separated into three stages. The growth of Ge on the PAA surface begins between pores (figure 3(a)). The separated cells have an clear hexahedral form with a size corresponding to that of the matrix cells. Further deposition leads to the overgrowth of the germanium cells (figure 3(b)) until they close over (figure 3(c)). A solid, fine-grain film is formed, and the surface of this film has all the features of the substrate. The process of growth of the Ge nanostructures deposited on matrices with a different porous structure is similar to the process described above.

As will be shown later, the height of the nanostructures depends on the pore diameter. The depth of penetration of germanium into the pore channels can reach a few microns. The EDX analysis of the cross section of the samples shows the presence of germanium to a depth of 2.5 μm from the surface of the matrix (figure 4), but it can be seen that the formation of nanostructures occurs at the thin layer near the surface.

The surface morphology was studied using SEM and AFM. The samples were fixed on a carbon tape and the matrix was selectively dissolved in 5% H_3PO_4. Deposition on PAA120^{bot}, PAA80^{bot} and PAA40^{bot} matrices leads to the formation, in the pore channels, of nanostructures in the form of rods. The size and distribution of these rods replicate the porous structure of the templates. Figure 5 shows SEM and AFM micrographs of the Ge nanostructure arrays and their structural parameters, i.e. the diameters and distances between rods. In the 3D AFM pictures, due the influence of the shape of the probe, the rods are shown in the form of cones. This

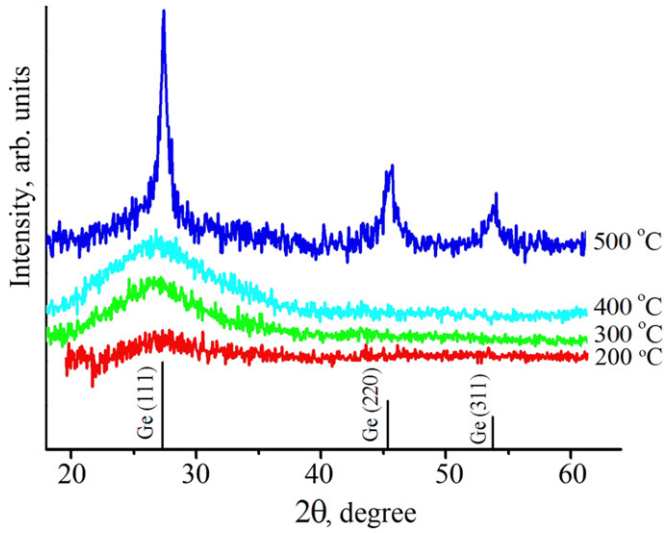

Figure 8. XRD patterns of the samples of Ge deposited on PAA120^{top} matrices at substrate temperatures of 200 °C, 300 °C, 400 °C and 500 °C. A gram bar shows JCPDS № 81683.

complicates the determination of the transverse dimensions of the nanostructures, but allows one to obtain their heights through the analysis of the height distribution histogram.

Deposition on the PAA40^{bot}_5 matrix with pore channels etched to 67 nm leads to the formation of nanostructures in the form of rings (figure 6). The external diameter corresponds to the average pore diameter, the internal diameter is 20 $\pm$ 3 nm and the height is 54 $\pm$ 5 nm. In this case the growth of the film on the PAA surface prevents the filling of pores which limits the penetration of germanium into the pores.

In the case of deposition on the PAA120^{top} matrix (figure 7) the relief provided by the first stage of anodization is inherited: large particles with small outgrowths are observed. The distances between the large particles correspond to the interpore distances for the matrix PAA120^{bot} whereas small outgrowths replicate the surface structure of the PAA120^{top} matrix. The average diameter of the outgrowths is 16 $\pm$ 3 nm and the average distance between them is 32 $\pm$ 6 nm. 5–10 small growths are present on one large particle.

So the formation of nanostructures by deposition on PAA matrices can be divided into two competing processes. The first process is the adhesion of germanium to the pore walls. This process leads to the overgrowth of pores towards their centers. The second process is the growth of the germanium film on the surface of the matrix. This process leads to the closing of the pores and further formation of the film.

3.2. Structural studies

Figure 8 shows XRD patterns of the samples with Ge deposited on PAA120^{top} matrices. The XRD curves of the samples deposited at substrate temperatures lower than 400 °C show an amorphous halo only. For the sample deposited at 500 °C the diffraction peaks corresponding to the (111), (220) and (311) crystallographic plains appear. The calculation of the lattice constant (a = 5.647 $\pm$ 0.003 Å) shows a decrease of its value in comparison to the crystallographic data for germanium (5.658 Å, JCPDS № 81683). Nevertheless the calculation gives the broadening caused by the scattering on blocks with an average size of 11.2 $\pm$ 1.9 nm.

Figure 9 shows the Raman spectra of the samples mentioned above in the XRD section. For comparison, a spectrum for bulk germanium is presented. Under normal conditions, the frequency of transverse optical (TO) phonons ω is 300 cm^{-1} [17]. The spectrum recorded for the sample deposited at the temperature of 300 °C has a wide peak with a maximum of 275 cm^{-1}. The position of this peak corresponds to the amorphous state of Ge [6, 18]. But, in contradiction to the XRD results, in the Raman spectrum for the sample obtained at the substrate temperature of 400 °C partial crystallization is observed. The peak maximum is shifted to 298 cm^{-1}. The form of this peak has a significant asymmetry that allows the allocation of amorphous and crystalline phases by Gauss curve approximation (see the inset of figure 9).

For the sample deposited at the substrate temperature of 500 °C the asymmetry of the TO peak is negligible but the maximum is shifted in comparison to bulk Ge to a lower frequency by 2 cm^{-1}. The FWHM is 8 cm^{-1}. According to the theoretical calculations made by Wellner *et al* [19] for Ge nanocrystals in a SiO_2 matrix, the negative shift and peak broadening can be caused by the phonon confinement effect. So in our case the Ge nanocrystals are not stressed and have an average size of about 10 nm.

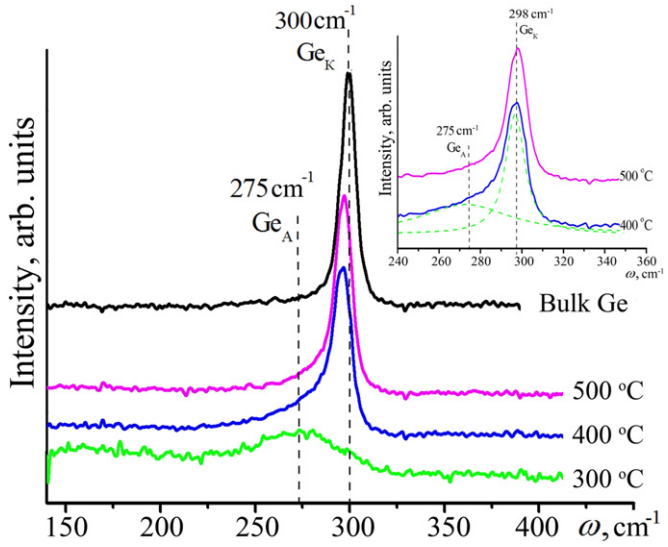

Figure 9. Raman spectra of the samples of Ge deposited on PAA120^{top} matrices at substrate temperatures of 300 °C, 400 °C and 500 °C in comparison to bulk Ge. The inset shows the allocation of amorphous and crystalline phases by Gauss approximation to the spectrum of the sample obtained at 400 °C.

4. Conclusion

Using the method of anodic oxidation, we have obtained matrices of PAA with different porous structure parameters. The pore diameters and the distances between them are set by the anodization potential. The best ordering of pores is observed for the bottom of matrices grown at 40 V. These matrices were used as the templates for the growth of germanium nanostructures. These can be obtained in the form of rods and rings. The formation of nanostructures can be divided into two competing processes: the adhesion of germanium to the pore walls, which leads to the overgrowth of pores towards their centers, and the growth of germanium film on the surface of the matrix, which leads to the closing of the pores and further to formation of a film.

The investigation of the structure using XRD and Raman spectroscopy shows germanium crystallization at a substrate temperature of 500 °C. Deposition at the temperatures less 300 °C leads to germanium in the amorphous state. Samples obtained at 400 °C are in a mixed amorphous–crystalline state. The Ge crystal sizes estimated from the Raman results are in good agreement with the values obtained from the XRD study.

Acknowledgments

Part of this work (the development of the thermal deposition processes) was supported by Russian Scientific Fund (Grant No. 15-19-10002). The authors would like to thank the researchers of the Materials Science Department of Lomonosov's Moscow State University for their help with the SEM investigations.

References

[1] Ray S K, Das S, Singha R K, Manna S and Dha A 2011 Structural and optical properties of germanium nanostructures on Si(100) and embedded in high-*k* oxides *Nanoscale Res. Lett.* **6** 224
[2] Parola S, Quesnel E, Muffato V, Bartringer J and Slaoui A 2013 Influence of the embedding matrix on optical properties of Ge nanocrystals-based nanocomposite *J. Appl. Phys.* **113** 053512
[3] Giri P K, Bhattacharyya S, Kesavamoorthy R, Panigrahi B K and Nair K G M 2009 Intense ultraviolet–blue photoluminescence from SiO_2 embedded Ge nanocrystals prepared by different techniques *J. Nanosci. Nanotechnol.* **9** 1–7
[4] D'Azevedo W M Jr, da Silva E F, de Vasconcelos E A and Boudinov H 2005 Visible photoluminescence from Ge nanoclusters implanted in nanoporous aluminum oxide films *Microelectron. J.* **36** 992–4
[5] Cosentino S, Mirabella S, Miritello M, Nicotra G, Savio R L, Simone F, Spinella C and Terras A 2011 The role of the surfaces in the photon absorption in Ge nanoclusters embedded in silica *Nanoscale Res. Lett.* **6** 135
[6] Buljan M, Pinto S R C, Rolo A G, Martin-Sanchez J, Gomes M J M, Grenzer J, Mucklich A, Bernstorff S and Holy V 2010 Self-assembling of Ge quantum dots in an alumina matrix *Phys. Rev.* B **82** 235407
[7] Maeda Y, Tsukamoto N and Yazawa Y 1991 Visible photoluminescence of Ge microcrystals embedded in SiO_2 glassy matrices *Appl. Phys. Lett.* **59** 3168–70
[8] Hayashi R, Yamamoto M, Tsunetomo K, Kohno K, Osaka Y and Nasu H 1990 Preparation and properties of Ge microcrystals embedded in SiO_2 glass films *Japan. J. Appl. Phys.* **29** 756–9

[9] Das S, Singha R K, Dhar A, Ray S K, Anopchenko A, Daldosso N and Pavesi L 2011 Electroluminescence and charge storage characteristics of quantum confined germanium nanocrystals *J. Appl. Phys.* **110** 024310
[10] Zhan W, Huangfu Y, Fang X, Hong X, Xia L, Guo X and Ye H 2013 Selective epitaxial growth of Ge nanodots with ultra-thin porous alumina membrane *Chin. Opt. Lett.* **11** S10206
[11] Masuda H, Yada K and Osaka A 1998 Self-ordering of cell configuration of anodic porous alumina with large-size pores in phosphoric acid solution *Japan. J. Appl. Phys.* **37** L1340–2
[12] Thompson G E 1997 Porous anodic alumina fabrication, characterization and applications *Thin Solid Films* **297** 192–201
[13] Petukhov D I, Napolskii K S, Berekchiyan M V, Lebedev A G and Eliseev A A 2013 Comparative study of structure and permeability of porous oxide films on aluminum obtained by single- and two-step anodization *Appl. Mater. Interfaces* **5** 7819−7824
[14] Mei Y F, Li Z M, Chu R M, Tang Z K, Siu G G, Fu R K Y, Chu P K, Wu W W and Cheah K W 2005 Synthesis and optical properties of germanium nanorod array fabricated on porous anodic alumina and Si-based templates *Appl. Phys. Lett.* **86** 021111
[15] Valeev R G, Beltukov A N, Vetoshkin V M, Surnin D V, Bakieva O R and Khohryakov S V 2010 Modernization of the sample preparation chamber of LAS-2000 device for thin films deposition in the ultra-high vacuum conditions *Vac. Tech. Technol.* **20** 235–40 (in Russian)
[16] Shelekhov E V and Sviridova T A 2000 Programs for x-ray analysis of polycrystals *Met. Sci. Heal Treat.* **42** 309–13
[17] Milekhin A G, Varavin V V, Nikiforov A I, Pchelyakov O P, Maev D E, Vogel N and Zahn D R T 2006 Micro-Raman scattering by laser-modified structures with Ge/Si quantum dots *Phys. Solid State* **48** 2183–6
[18] Williams G M, Bittar A and Trodahl H J 1990 Crystallization and diffusion in progressively annealed a-Ge/SiO_x superlattices *J. Appl. Phys.* **67** 1874–8
[19] Wellner A, Paillard V, Bonafos C, Coffin H, Claverie A, Schmidt B and Heinig K H 2003 Stress measurements of germanium nanocrystals embedded in silicon oxide *J. Appl. Phys.* **94** 5639–42